Russian Journal of Earth Sciences, Vol. 23, ES1001
https://doi.org/10.2205/2022ES000822

Experiment with the X-band radar at the Nizhny Novgorod cable car: First Results

K. Ponur *,[1], Yu. Titchenko[1], V. Karaev[1], E. Meshkov[1], M. Panfilova[1], I. Lebedev[1], A. Krylov[2], and E. Khakin[3]

[1] *Institute of Applied Physics RAS, Nizhny Novgorod, Russia*
[2] *JSC "Nizhegorodskie Ropeways", Nizhny Novgorod, Russia*
[3] *EFT-GROUP, Moscow, Russia*

Received 13 October 2022; accepted 6 December 2022; published 7 February 2023.

The first results of data processing of the experiment on the Nizhny Novgorod cable car are presented. A pulsed X-band radar was installed on a technological trolley and performed measurements while moving in two modes that worked sequentially. In the radio altimeter mode, the reflected waveform was measured and the distance to the scattering surface was determined. In the Doppler mode, the Doppler spectrum of the reflected signal was measured, which contains information about the statistical parameters of the surface. Data processing was carried out and the first results confirmed the assumption that the Doppler spectrum can be an effective tool for classifying the type of the underlying surface according to the "ice/water" criterion. Subsequent data processing will allow us to evaluate the accuracy of the developed algorithms.

Keywords: quasi-specular scattering, nadir sounding, water and ice Doppler spectra, reflected pulse waveform, experiment, x-band radar

Citation: Ponur, K., Yu. Titchenko, V. Karaev, E. Meshkov, M. Panfilova, I. Lebedev, A. Krylov, and E. Khakin (2023), Experiment with the X-band radar at the Nizhny Novgorod cable car: First Results, *Russian Journal of Earth Sciences*, Vol. 23, ES1001, doi: 10.2205/2022ES000822.

1 Introduction

One of the most effective methods of remote sensing of the sea surface is radar sounding. Placing radars on satellites makes it possible to obtain operational and global information, in particular, on the wave parameters and the surface wind field, regardless of the time of day and cloudiness. The most well-known orbital radars are scatterometers that measure the near-water wind field [*Brennan et al.*, 2009; *Quilfen et al.*, 2001; *Ricciardulli and Wentz*, 2015; *Rivas et al.*, 2014; *Stoffelen et al.*, 2017], radio altimeters that measure the significant wave height, wind speed and the mean sea level [*Elfouhaily et al.*, 1998; *Freilich and Challenor*, 1994; *Karaev et al.*, 2002; *Lillibridge et al.*, 2014] and synthetic aperture radars (SAR) that have high spatial resolution [*Fisher et al.*, 2008; *Furevik and Korsbakken*, 2000; *Horstmann et al.*, 2000; *Shen et al.*, 2014].

Growing requirements for expanding the number of measured parameters incentivize development of new radar equipment. It is planned to install a Ku-band radar on the promising Russian oceanographic satellite "Ocean", which will perform measurements in a channel near nadir sounding [*Karaev et al.*, 2010, 2018]. It will be the first orbital radar that performs measurements in two modes:

- during nadir sounding, measurements are performed in the radio altimeter mode and the significant wave height along the flight direction is retrieved;
- in the scanning mode (±13 deg.), a radar image of the surface is formed and the field of the mean square slopes (MSS) of large-scale in comparison with radar wavelength, sea waves is retrieved [*Karaev et al.*, 2021b; *Panfilova et al.*, 2020]. The frequency of switching between modes and their duration are chosen so as to form a full radar coverage of the sea surface (without gaps).

*Corresponding author: ponur@ipfran.ru

The measurement scheme is shown in Figure 1. Due to the use of knife-like antenna beam (1.5° × 30°) at an altitude of 500 km, each spatial element (14 km×14 km) in a 230 km swath will be observed for more than 30 seconds. This has never been done before.

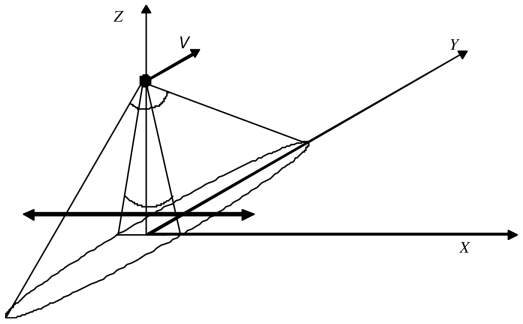

Figure 1: Radar measurement scheme.

2 Developed radar with knife-like antenna beam

In contrast to the middle incidence angles, measurements at small incidence angles are difficult to implement in the course of a field experiment. One of the options for solving the problem is to install a radar on the bridge, and such a measuring complex was installed on the metro bridge across the Volga River (Nizhny Novgorod) to measure the current velocity. In the experiment, the Doppler spectrum of the reflected radar signal was measured and the dependence of the Doppler spectrum parameters on the angle of incidence and azimuthal angle was studied [*Karaev et al.*, 2021a; *Ryabkova et al.*, 2020]. However, the measurements were performed from an immobile carrier and only in the Doppler mode.

The possibility of measuring from an airplane is discussed in the following papers [*Nekrasov et al.*, 2013, 2017]. However, the experiment was not carried out in these works. Installing a radar on an airplane is a technically difficult task. So, a different way was chosen for carrying out "flight" tests.

To carry out the experiments, JSC "Micran" [*Micran JSC*, 2022] developed and manufactured an X-band radar by order of the IAP RAS. Measurements in altimeter and Doppler modes are performed in a cycle of 10.285 s (0.285 s and 10 s). On Figure 2 shows a photo of the radar. The electronics are inside in a metal box rigidly connected to the antenna (knife-like antenna beam), which is on the top in the figure.

The scan mode wasn't implemented due to the complexity of the design, so the Doppler mode will also be tested in nadir sounding. Radar parameters are given in Table 1.

Figure 2: Photo of the X-band knife-like antenna beam (30° × 3.6°).

The radar operates in two modes, and in order to test them, it is necessary to fulfill a number of requirements for the measurement scheme.

The Doppler spectrum of the reflected radar signal contains information about the distribution of the radial component of the surface velocity. For ice or land, there is no proper surface motion, so measurements must be made from a moving carrier to test the Doppler mode.

The altimeter mode measures the significant wave height. Wind waves on the river have a small height. The range resolution is about 50 cm, so it will be extremely difficult to test algorithms for measuring wave height.

The best option for measuring and testing both modes was the installation of a radar in the technological trolley of the Nizhny Novgorod cable car. The first experiment was performed on December 2, 2020. The news show "Vesti Povolzhya" aired a piece about it [*Vesti*, 2022].

Table 1: Parameters of the X-band radar manufactured by Micran JSC

Carrier frequency	9.2–9.5 GHz
Frequency deviation	289.99 MHz
Beamwidth	30° × 3.6°
Output power	1 W
Pulse duration	2.85 ms
Output data	Doppler spectrum Reflected pulse waveform

3 Experiment at the Nizhny Novgorod cable road

The experiment was conducted on December 4, 2021. The cable car passed over the Grebnoy Kanal (Grebnoy Channel), an enclosed reservoir (see Fig-

ure 3) that is located near the higher bank of the Volga River.

The first substruction of the Nizhny Novgorod cable car is located on a small river island (see Figure 3). By the time the experiment was started, an ice cover had formed over the Grebnoy Kanal, and the Volga River has not yet frozen, so when the technological trolley moved, the measurements were carried out over the ice cover (Grebnoy Kanal) and the open water surface (Volga River).

To carry out the experiment with the new radar for the first time, a data processing software package was developed. Detailed analysis and comparison of model estimates for the ice cover and the water surface deserves a separate publication on each mode of operation of the radar and will be carried out in the future. In this paper, we give examples of processing for the Doppler and altimeter modes of the radar.

The installation of the radar on the technological trolley of the Nizhny Novgorod cable car ensures the movement of the radar over the water surface and ice, which makes it possible to test the Doppler mode.

The trolley moves along a rope that sags between the supports. As a result, movement is "simulated" over an "rough" surface. This can be interpreted as moving over a "large-scale" wave. The height of the "wave" can be chosen by setting the average time of the reflected pulses and knowing (measuring) the change in the coordinates of the technological trolley. Thus, it is possible to test the radio altimeter mode.

Figure 4 shows the change in the height of the technological trolley, measured by the geodetic receivers of navigation signals during the experiment. The measurements began on the lower bank at the Bor station and continued during the ascent to the higher bank at the Nizhny Novgorod station. The height difference is about 80 m. GNSS receiver measures altitude relative to sea level.

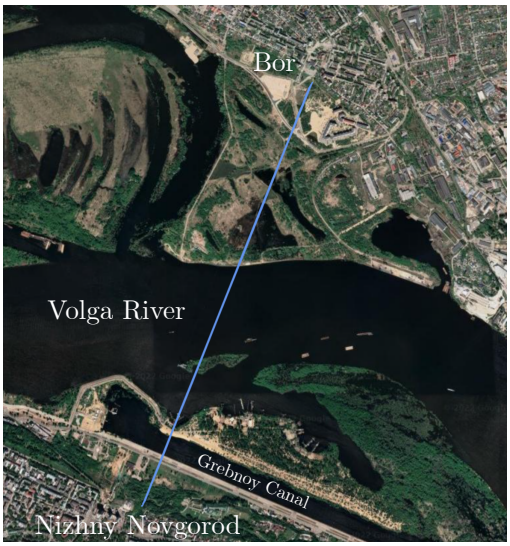

Figure 3: The scheme of the experiment. Cable car shown as a straight line. In the south of the track is the Nizhny Novgorod station. In the north is Bor station.

During the experiment, three full laps were made during which the orientation of the antenna relative to the direction of movement of the radar and the operating modes changed. The duration of the lap is about 30 minutes. The radar installed on the technological trolley is shown in Figure 5.

"Household" GNSS receivers measure the height and speed of movement with a large error, therefore, to ensure the required accuracy, the EFT M1 Plus geodetic receiver manufactured by EFT-GROUP (Moscow) was used. It provides a measurement accuracy of about 2–4 cm. Employees of the company took part in the experiment and prepared the data for further processing.

4 Data processing

The data is currently being processed. The first results are shown below. In radio altimeter mode, a short pulse is emitted. Due to the frequency deviation of about 300 MHz, a range resolution of about 50 cm is achieved. The height of the radar above the reflecting surface can be calculated by measuring the propagation time of an electromagnetic wave from the radar to the reflecting surface and back. An example of reflected pulses is shown in Figure 6. The delay time has been converted to range and the reflected pulse plotted on the range axis (horizontal axis). On Figure 6a different colors show single pulses from a burst of 100 pulses (burst duration 0.285 s). The waveform of the reflected pulse varies greatly from pulse to pulse.

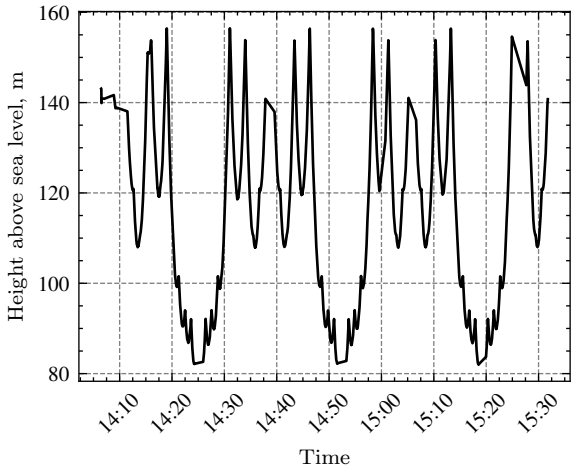

Figure 4: Changing the height of the technological trolley (radar) during the experiment.

Figure 5: Technological trolley with installed radar before the experiment.

Figure 6b shows the average pulse for the emitted burst. It has a stable waveform and can be used to restore the distance to the reflective surface. Time of repetition is approximately 10.285 s.

Doppler mode measures the spectral characteristics of the reflected signal and the movement of the radar results in a Doppler spectrum even for a stationary surface. The width of the Doppler spectrum depends on the velocity of the radar, the antenna beam and the parameters of the reflecting surface. An example of a Doppler spectrum calculated from a record with a duration of 0.7 s is shown in Figure 7. The red curve corresponds to a Gaussian with mean and variance calculated from the measured Doppler spectrum. The measured Doppler spectrum aligns well with the modeled one, and it will be possible to use the developed processing algorithms to restore the statistical characteristics of the scattering surface.

The radar looks down vertically and the observed Doppler spectrum shift is associated with the movement of the technological trolley between the supports. Sagging of the rope leads to the appearance of a vertical velocity component. In this case, the movement is up (technological trolley approaches the support) or down (moves away). The width of the Doppler spectrum depends on the velocity vector and the width of the antenna pattern. The coordinates of the technological trolley were recorded simultaneously by the geodetic receiver EFT M1 Plus. In the future, the reconstructed height will be compared according to the radar data with the measurements of the geodetic receiver. In addition, it will be possible to classify the type of underlying surface (land, ice, water) and compare Doppler spectra.

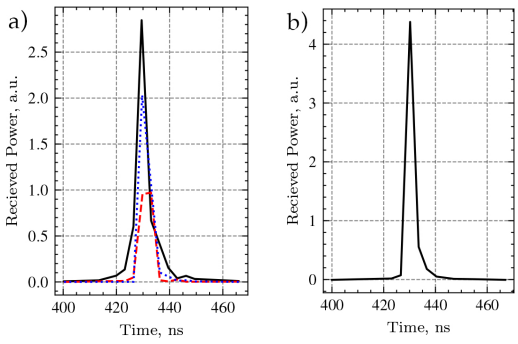

Figure 6: An example of a reflected pulse: a) single reflected pulses; b) average pulse. The height of the technological trolley is about 64.5 m.

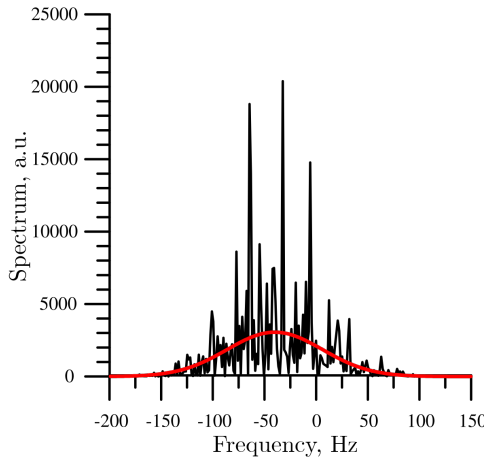

Figure 7: Doppler spectrum of the reflected signal: black curve – measured Doppler spectrum, red curve – Gaussian model. Time record is 0.7 s.

5 Discussion

On Figure 8 examples of average reflected impulses (averaging time 0.285 ms) when moving technological trolley over the Volga river (open water) are presented. During processing, the pulses were numbered and the time interval between adjacent pulses is 10.285 s. The observed momentum shift with increasing number is due to the lifting of the technological trolley when approaching a substruction located on the island.

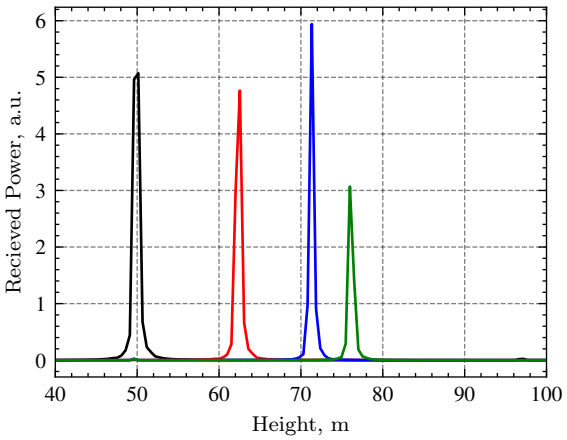

Figure 8: Changing the position of the pulse when moving over the Volga River.

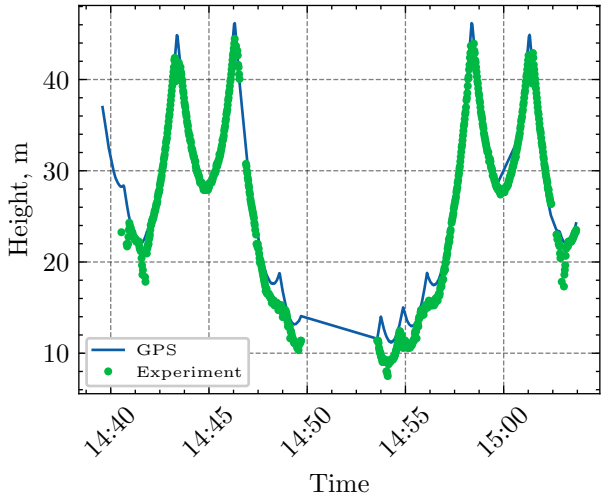

Figure 9: Dependence of the height of the technological trolley on time: GNSS is solid line, radar data is dots.

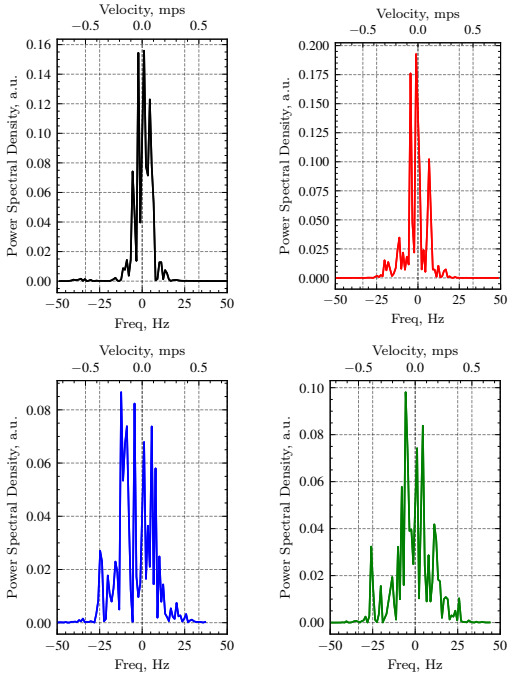

Figure 10: Examples of Doppler spectra of the reflected radar signal.

The GNSS receiver measures the height of the cart relative to sea level, and the radar measures distance from the technological trolley to the reflective surface. Therefore, when plotting Figure 9 height (from GNSS) and distance to surface (from radar) were combined in the first maximum. The difference was calculated and this made it possible to go from the distance measured by the radar to the height of the trolley (radar) point above sea level, measured by GNSS.

You can see a good match, and quantitative estimates will be obtained after processing is completed and presented in the next article on the altimeter mode.

In the second mode, the radar measured the Doppler spectrum of the reflected signal. For the same cycles measurements (see Figure 8), the Doppler spectra were calculated and presented in Figure 10.

For nadir sounding and horizontal motion, the DS shift should be equal to zero. The appearance of a bias usually says that there is a vertical velocity component. This also affects the width of the Doppler spectrum.

Now consider the change in the Doppler spectrum upon transition from one type of underlying surface to another. As shown in [*Karaev et al.*, 2022a,b], Doppler spectrum can significantly change its parameters when moving from the ice cover to the water surface if the knife-like antenna pattern is oriented along the direction of travel. For ease of comparison, the spectra were normalized.

Figure 11 shows a comparison of the measured Doppler spectra with the duration of 1 s that are smoothed by a moving average with a window of 0.97 Hz. The black curve is the Doppler spectra from the water surface and the blue curve is from the ice cover.

It can be seen that the Doppler spectrum reflected from the water surface is wider than the Doppler spectrum measured on the ice cover. This is explained by the fact that the roughness of the ice cover (MSS) is significantly less than the roughness of the surface waves.

As is known, at small angles of incidence, the dominant backscattering mechanism is quasi-specular. Reflection occurs from areas of the surface oriented perpendicular to the incident radiation. The width of the Doppler spectrum depends on the velocity carrier motion. The Doppler spectrum over the water surface is wider than over the ice because MSS of waves is larger and the reflected signal is collected from a larger area and the interval of incidence angles involved in the formation of the reflected signal will be more. This result in more spread radial velocities and the width of the Doppler spectrum will be greater for the water surface.

Let's consider another interesting effect that was studied in the experiment. It is associated with orientation of the antenna pattern relative to the direction of movement. During the experiment measurements were performed for two antenna pattern orientations:

1. knife-like antenna beam was oriented along the direction of movement;

2. knife-like antenna beam was oriented across the direction of movement.

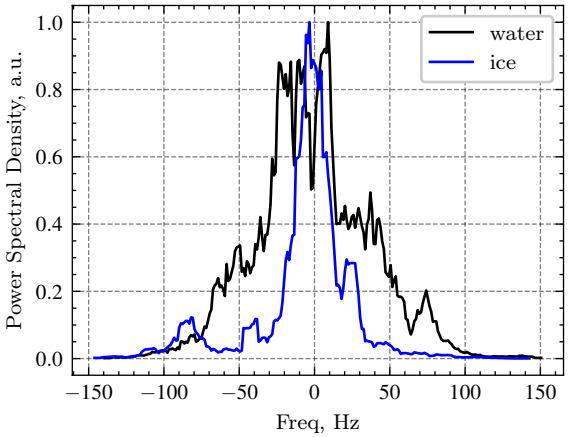

Figure 11: An example of Doppler spectra reflected from the water surface (black curve) and from the ice cover (blue curve).

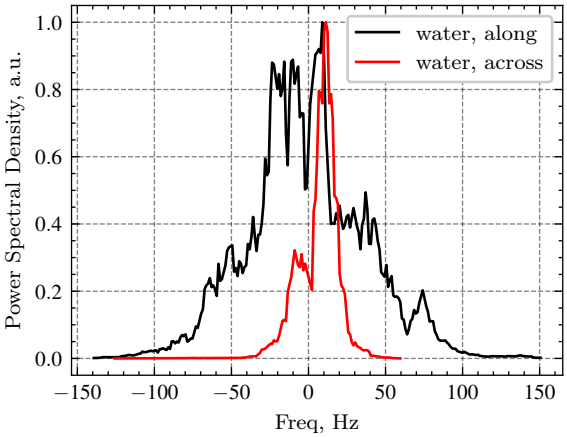

Figure 12: Doppler spectra of the reflected radar signal over the water surface for orienting the knife-like antenna across the direction of movement (red curve) and along the direction of travel (black curve).

The orientation of the antenna will not affect the shape of the reflected pulse, but the orientation is important for Doppler spectrum. For an example, see Figure 12. Black curve corresponds case the footprint was oriented along the direction of motion, and red curve corresponds case the footprint was oriented across movement. This result confirms the theoretical conclusions of [*Karaev et al.*, 2022a,b].

6 Conclusions

The paper discusses setting up and conducting the first experiment with an X-band pulsed radar on the Nizhny Novgorod cable road. The radar operated in two modes: 1) altimeter mode and 2) Doppler mode.

A set of programs for data processing has been developed and the first results of processing are being discussed.

In the first mode, the waveform of the reflected pulse is measured, the propagation time of the electromagnetic wave from the radar to the scattering surface (two way) is determined, and the distance is calculated. The range resolution is about 0.5 m.

In the second mode, the Doppler spectrum of the reflected radar signal is measured, and independent information about the movement velocity (GNSS receiver), it will be possible to retrive the MSS of the large-scale surface waves.

Data processing and subsequent comparison with GNSS data showed that in the altimeter mode the distance from the radar to the reflecting surface is successfully measured.

An analysis of the Doppler spectra showed that the width of the Doppler spectrum is a reliable indicator of the type of underlying surface.

This paper presents the first results of experimental data processing. In the course of further research, quantitative estimates of the accuracy of algorithms will be obtained and compared with the developed models of the Doppler spectrum.

Acknowledgment

This work is supported by Russian Science Foundation (grant 20-17-00179).

We would like to thank JSC "Micran" for developing and manufacturing X-band radar. We appreciate JSC "Nizhegorodskie Ropeways" for their help in setting up the experiment and conducting it. Likewise, we express our gratitude to the staff of the Nizhny Novgorod branch of the company "EFT-GROUP" for participating in the experiment and performing measurements by GNSS receiver.

References

Brennan, M. J., C. C. Hennon, and R. D. Knabb (2009), The Operational Use of QuikSCAT Ocean Surface Vector Winds at the National Hurricane Center, *Weather and Forecasting*, *24*(3), 621–645, doi:10.1175/2008waf2222188.1.

Elfouhaily, T., D. Vandemark, J. Gourrion, and B. Chapron (1998), Estimation of wind stress using dual-frequency TOPEX/POSEIDON data, *103*(11), 25,101–25,108.

Fisher, C. M., G. S. Young, N. S. Winstead, and J. D. Haqq-Misra (2008), Comparison of Synthetic Aperture Radar–Derived Wind Speeds with Buoy Wind Speeds along the Mountainous Alaskan Coast, *Journal of Applied Meteorology and Climatology*, *47*(5), 1365–1376, doi:10.1175/2007jamc1716.1.

Freilich, M. H., and P. G. Challenor (1994), A new approach for determining fully empirical altimeter

wind speed model functions, *Journal of Geophysical Research*, *99*(C12), 25,051, doi:10.1029/94jc01996.

Furevik, B., and E. Korsbakken (2000), Comparison of derived wind speed from synthetic aperture radar and scatterometer during the ERS tandem phase, *IEEE Transactions on Geoscience and Remote Sensing*, *38*(2), 1113–1121, doi:10.1109/36.841990.

Horstmann, J., W. Koch, S. Lehner, and R. Tonboe (2000), Wind retrieval over the ocean using synthetic aperture radar with C-band HH polarization, *IEEE Transactions on Geoscience and Remote Sensing*, *38*(5), 2122–2131, doi:10.1109/36.868871.

Karaev, V., M. Kanevsky, M. Meshkov, and E. Kovalenko (2010), The concept of the advanced space microwave radar for remote sensing of the ocean at small incidence angles, p. 23, National Taiwan Ocean University, Keelung, Taiwan.

Karaev, V., M. Panfilova, Y. Titchenko, E. Meshkov, and M. Ryabkova (2018), Experiment at the International Space Station: a microwave radar with scanning fan beam antenna at nadir probing, pp. 232–233, 25 years of Progress in Radar Altimetry symposium, Ponta Delgata, Portugal.

Karaev, V., M. Ryabkova, M. Panfilova, Y. Titchenko, E. Meshkov, and E. Zuikova (2021a), Microwave Doppler Radar Experiment on a River, in *2021 IEEE International Geoscience and Remote Sensing Symposium IGARSS*, pp. 7350–7353, IEEE, doi:10.1109/igarss47720.2021.9554820.

Karaev, V., K. Ponur, M. Panfilova, Y. Titchenko, M. Ryabkova, and E. Meshkov (2022a), Radar Sensing of SEA ICE at the Small Incidence Angles: Simulation and Comparison of the Different Approaches, *IGARSS*, doi:10.1109/igarss46834.2022.9883231.

Karaev, V., Y. Titchenko, M. Panfilova, M. Ryabkova, E. Meshkov, and K. Ponur (2022b), Application of the Doppler Spectrum of the Backscattering Microwave Signal for Monitoring of Ice Cover: A Theoretical View, *Remote Sensing*, *14*(10), 2331, doi:10.3390/rs14102331.

Karaev, V. Y., M. B. Kanevsky, G. N. Balandina, P. D. Cotton, P. G. Challenor, C. P. Gommenginger, and M. A. Srokosz (2002), On the problem of the near ocean surface wind speed retrieval by radar altimeter: A two-parameter algorithm, *International Journal of Remote Sensing*, *23*(16), 3263–3283, doi:10.1080/01431160110075587.

Karaev, V. Y., M. A. Panfilova, M. S. Ryabkova, Y. A. Titchenko, E. M. Meshkov, and X. Li (2021b), Retrieval of the two-dimensional slope field by the SWIM spectrometer of the CFOSAT satellite: discussion of the algorithm, *Russian Journal of Earth Sciences*, *21*(6), 1–9, doi:10.2205/2021es000784.

Lillibridge, J., R. Scharroo, S. Abdalla, and D. Vandemark (2014), One- and Two-Dimensional Wind Speed Models for Ka-Band Altimetry, *Journal of Atmospheric and Oceanic Technology*, *31*(3), 630–638, doi:10.1175/jtech-d-13-00167.1.

Micran JSC (2022), Research and Production company Micran Joint Stock Company, https://www.micran.com/, Accessed: October 2, 2022.

Nekrasov, A., J. Ouellette, N. Majurec, and J. T. Johnson (2013), A Study of Sea Surface Wind Vector Estimation From Near-Nadiral Cross-Track-Scanned Backscatter Data, *IEEE Geoscience and Remote Sensing Letters*, *10*(6), 1503–1506, doi:10.1109/lgrs.2013.2261047.

Nekrasov, A., A. Khachaturian, V. Veremyev, and M. Bogachev (2017), Doppler Navigation System with a Non-Stabilized Antenna as a Sea-Surface Wind Sensor, *Sensors*, *17*(6), 1340, doi:10.3390/s17061340.

Panfilova, M., V. Karaev, L. Mitnik, Y. Titchenko, M. Ryabkova, and E. Meshkov (2020), Advanced View at the Ocean Surface, *Journal of Geophysical Research: Oceans*, *125*(11), doi:10.1029/2020jc016531.

Quilfen, Y., B. Chapron, and D. Vandemark (2001), The ERS Scatterometer Wind Measurement Accuracy: Evidence of Seasonal and Regional Biases, *Journal of Atmospheric and Oceanic Technology*, *18*(10), 1684–1697, doi:10.1175/1520-0426(2001)018<1684:teswma>2.0.co;2.

Ricciardulli, L., and F. J. Wentz (2015), A scatterometer geophysical model function for climate-quality winds: QuikSCAT ku-2011, *Journal of Atmospheric and Oceanic Technology*, *32*(10), 1829–1846, doi:10.1175/jtech-d-15-0008.1.

Rivas, M. B., A. Stoffelen, and G.-J. van Zadelhoff (2014), The Benefit of HH and VV Polarizations in Retrieving Extreme Wind Speeds for an ASCAT-Type Scatterometer, *IEEE Transactions on Geoscience and Remote Sensing*, *52*(7), 4273–4280, doi:10.1109/tgrs.2013.2280876.

Ryabkova, M., V. Karaev, M. Panfilova, Y. Titchenko, E. Meshkov, and E. Zuikova (2020), Doppler spectrum of backscattered microwave signal: experiment at the river, *Sovremennye problemy distantsionnogo zondirovaniya Zemli iz kosmosa*, *17*(5), 213–227, doi:10.21046/2070-7401-2020-17-5-213-227.

Shen, H., W. Perrie, Y. He, and G. Liu (2014), Wind speed retrieval from VH dual-polarization RADARSAT-2 SAR images, *IEEE Transactions on Geoscience and Remote Sensing*, *52*(9), 5820–5826, doi:10.1109/tgrs.2013.2293143.

Stoffelen, A., et al. (2017), Scientific Developments and the EPS-SG scatterometer, *IEEE Journal of selected topics in Applied Earth Observations and Remote Sensing*, *10*(5), 2086–2097, doi:10.1109/jstars.2017.2696424.

Vesti (2022), Radar for a fire aircraft is being developed by specialists from Nizhny Novgorod, Russian news channel, https://vestinn.ru/news/society/195732/.